Carbon 196 (2022) 493–498

Contents lists available at ScienceDirect

Carbon

journal homepage: www.elsevier.com/locate/carbon

Millimeter wave phased array antenna based on highly conductive graphene-assembled film for 5G applications

Shaoqiu Jiang [a,1], Rongguo Song [a,**,1], Zelong Hu [a], Yitong Xin [a], Guan-Long Huang [b], Daping He [a,*]

[a] Hubei Engineering Research Center of RF-Microwave Technology and Application, Wuhan University of Technology, Wuhan, 430070, China
[b] School of AI - Guangdong & Taiwan, Foshan University, Foshan, Guangdong, 528225, China

ARTICLE INFO

Keywords:
Graphene-assembled film
Millimeter wave
5G
Phased array
Beamforming

ABSTRACT

In the millimeter wave communication frequency band of 5G and coming 6G, the numbers of wireless electronic device will explosively grow. With the commitment of long-term carbon neutrality from various countries, metal replacement in millimeter wave antennas has become an urgent task to meet the requirements of green and sustainable development for the upcoming 5G era. In this paper, for the first time, phased array antennas (PAAs) based on highly conductive graphene-assembled film (GAF) were proposed for 5G millimeter wave applications with the advantages of light weight and high thermal conductivity. We designed and fabricated two PAAs of four-beam directional scanning phased array antenna (DSPAA) and continuous beam scanning phased array antenna (CSPAA). GAF linear antenna array has 212.5% wider operating bandwidth and 5 dB lower side lobes compared to the copper linear array. Based on GAF linear array and Butler matrix feed network, the GAF DSPAA was designed to work at 26 GHz. The GAF DSPAA has four beams with different directions at −28°, −8°, 6° and 22° respectively, showing excellent beam pointing performance. Furthermore, the GAF CSPAA demonstrated the ability to work in a satisfactory beam coverage ranging from −28° to 28°, and achieved a maximum radiation gain of 25.53 dBi at 26 GHz.

1. Introduction

The low frequency band (Sub-6G) of fifth-generation (5G) mobile communication has entered large-scale commercial deployment in various countries around the world [1]. As an important capacity supplement and capability improvement method, 5G millimeter wave communication technology has become the research focus of mobile communication [2–4]. At the same time, according to the evolution cycle of the mobile communication system, research on sixth-generation (6G) mobile communication technology is under consideration and planning [5–7]. For now, researchers have diverse vision for 6G, such as extremely low-power communications (ELPC), long-distance and high-mobility communications (LDHMC), and space-air-ground-sea integrated communications (SIC), etc. But in general, it will need the support of key technologies in 5G such as millimeter wave communication and Massive MIMO [8].

Phased array antenna is a key technology for target detection and autonomous driving environment perception [9–11]. In recent years, with flexible beam scanning and beamforming performance, millimeter wave phased array antennas have become an effective technical approach to realize Massive MIMO [12–15]. However, traditional antennas are mostly designed with metallic materials which suffer from high density, low thermal conductivity, poor corrosion resistance and mechanical stability. Especially in base-station communication, requirements on high-power handling, more functional and structural integration, and complicated deployment environment make metals face difficulties in heat dissipation and environmental reliability. Moreover, the mining and production of raw metallic materials can cause severe environmental pollution resource depletion [16–18]. Till now, more than 120 countries and regions around the world have put forward the goal of carbon neutrality with raising demands on environmentally sustainable development [19]. It is, thus, of far-reaching

* Corresponding author.
** Corresponding author.
E-mail addresses: rongguo_song@whut.edu.cn (R. Song), hedaping@whut.edu.cn (D. He).
[1] These authors contributed equally to this work.

https://doi.org/10.1016/j.carbon.2022.05.026
Received 8 January 2022; Received in revised form 7 May 2022; Accepted 11 May 2022
Available online 14 May 2022

significance and value to seek new materials for antenna fabrication as it is an important and heavily-used part in wireless communication systems.

As the first two-dimensional material discovered in the world [20], graphene has excellent electrical, thermal and mechanical properties [21–23]. Since its discovery, it has been applied to various fields such as biology, chemistry, medical science, and communication [24–27]. In our previous work, we prepared a graphene-assembled film (GAF) with high conductivity and realized the mass production. GAF has the advantages of light weight, flexibility, mechanical stability and high chemical stability compared with metal materials. Based on the GAF, various antenna structures have been designed, such as dipole antennas, microstrip antennas, wearable antennas, and single-beam millimeter wave antennas [28–32]. In addition, a four-beam directional scanning phased array based on the substrate integrated waveguide (SIW) Butler matrix was proposed [33]. However, the SIW-based feed network of the antenna is complicated in design, expensive to process and hard to realize continuous beam scanning.

In this work, we proposed two beam scanning phased array antennas based on highly conductive GAF for 5G mobile communication applications. We firstly designed a GAF linear array antenna working at 26.08 GHz, which conforms to the 5G NR communication frequency band proposed by World Radio Communication Conference 2019. The GAF linear array antenna has the measured −10 dB impedance bandwidth from 25.81 to 26.23 GHz. Based on the GAF linear array antenna, a GAF directional scanning phased array antenna (DSPAA) and a continuous beam scanning phased array antenna (CSPAA) are designed. The test results show that the four beams of DSPAA based on low cost microstrip Butler matrix point to −28°, −8°, 6°, and 22° respectively, and the beam of BSPAA can continuously scan in the range of −28°–28°. The proposed GAF multibeam and beam scanning phased array antenna in this work reveal its valuable prospects in 5G millimeter mobile communication. This research has broad prospects for 5G communication, radar, automotive driving and other typical millimeter wave applications requiring phased array antenna.

2. Characterization of graphene assembled film

The graphene-assembled film was fabricated in three steps [30]. Firstly, the graphene oxide (GO) suspension (purchased from Wuxi chenyi education technology Co. Ltd.) with the concentration of 15 mg/mL was uniformly coated on the polyethylene terephthalate (PET) substrate and dried at room temperature to obtain the free-standing GO-assembled film (GOAF). Secondly, the GOAF was annealed at 1300 °C for 2hrs and at 2850 °C for 1hr in argon (Ar) gas atmosphere. Finally, the large area GAF was prepared by a rolling compression process with 150 MPa pressure.

Fig. 1(a) shows the digital photo of free-standing GAF with a large area of 70 cm × 55 cm and the density of 1.59 g/cm^3, which is only 18% of copper (8.65 g/cm^3). The GAF can be folded in half three times, as shown in the illustration of Fig. 1(b), indicating that the GAF has excellent flexibility and mechanical stability. The conductivity of GAF is 1.1×10^6 S/m tested by Four-Probe Method. In Fig. 1(b), the Raman spectrum of GAF shows small D (1344 cm^{-1}) peak and sharp G (1582 cm^{-1}) peak, which proves GAF has less lattice defects and high conductivity. As shown in Fig. 1(c), the X-ray diffraction (XRD) pattern shows two characteristic graphitic peaks locate at $2\theta = 26.5°$ (002) and $2\theta = 54.7°$ (004), respectively. The two characteristic graphitic peaks indicate the interlayer spacing of graphene layer is 0.34 nm and also the high graphitization structure of GAF. The SEM image in the illustration of Fig. 1(c) shows the GAF with thickness of 23 μm has a regular stacking structure, which is consistent with the XRD results. In addition, Fig. 1(d) illustrates the infrared image of thermal conduction comparison of GAF and copper. The GAF has very high thermal conductivity compared with copper foil.

3. Results and discussion

3.1. GAF linear array antenna

In order to obtain high gain, narrow beam coverage and high directivity, a serially-fed 10-patch microstrip linear array antenna (LAA)

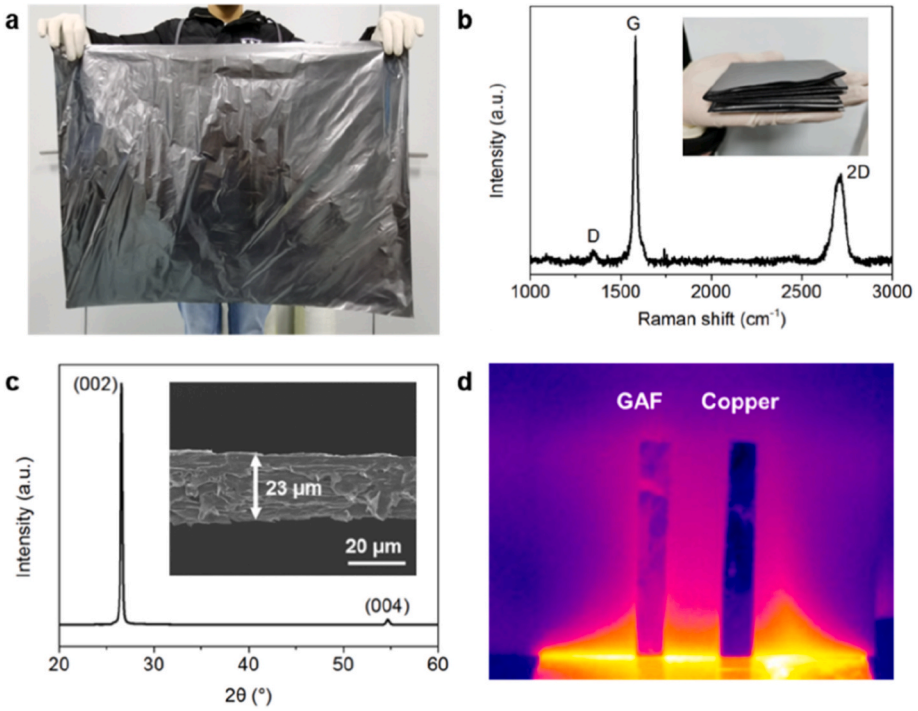

Fig. 1. (a) The digital photo of GAF with area of 70 cm × 55 cm; (b) The Raman spectrum after being folded in half three times (illustration) of GAF; (c) The XRD pattern and SEM image (illustration) of GAF; (d) Thermal conduction comparison of GAF and copper. (A colour version of this figure can be viewed online.)

is designed as the element of GAF phased array antenna. Fig. 2(a) shows the schematic diagram of the serially-fed GAF linear array. The GAF radiation patch (silver white part in Fig. 2(a)) is composed of 10 microstrip rectangular patches that meet the Taylor distribution in series. The length (l) of all patches is equal, which is the half equivalent wavelength of the working frequency in the dielectric substrate. The width is symmetric about the center of the GAF linear array, and satisfies the Taylor distribution of w1:w2:w3:w4:w5 = 0.27:0.44:0.67:0.88:1. Each patch is fed in series by a microstrip line along the *x*-axis direction. In order to ensure that the current phases of the elements of the microstrip patch linear array are equal, the length of the feed line with the characteristic impedance of 100 Ω is also selected to be half of the equivalent wavelength of the working frequency in the dielectric substrate. To match the 100-Ω microstrip line to the 50-Ω impedance of the input port, a quarter wavelength impedance converter is added to the left of the linear array. Rogers RT/duriod 5880 PCB with a thickness of 0.5 mm, dielectric constant of 2.2 and loss tangent of 0.0009 is selected as the dielectric substrate (the gray part in Fig. 2(a)). The structure is modelled and simulated in the CST Studio. After parametric optimization, the structural parameters of the GAF microstrip LAA are shown in Table S1. In addition, the current intensity distribution of the GAF LAA at 26 GHz is shown in Fig. S1. The maximum current density is in the center patch of the LAA, and the patches of two sides are sequentially weakened, which has high symmetry. Fig. 2(b) shows the digital photo of the optimized GAF antenna produced by the laser engraving method. A 2.92 mm coaxial connector is used to facilitate instrument testing. The vector network analyzer (Keysight N5247A) is used to test the performances of GAF LAA. For comparison, the same copper LAA is fabricated (shown in Fig. S2) and measured using the same method. Fig. 2(c) depicts reflection coefficient results of GAF and copper LAA. The GAF LAA resonates at 26 GHz with the reflection coefficient of −39 dB, which conforms to the 5G NR communication frequency band proposed by World Radio Communication Conference 2019. The measured −10 dB impedance bandwidth is 25.79–26.3 GHz, which is 212.5% of that of copper antenna's 25.92–26.16 GHz. This is because each GAF antenna element has a lower Q value than the copper element, resulting in a wider bandwidth of the overall array antenna. To further demonstrate the radiation performance of the GAF microstrip linear array, the measured H-plane and E-plane normalized radiation pattern of GAF and copper LAA are shown in Fig. S3 and Fig. 2(d), respectively. With comparing the H-plane radiation pattern of GAF LAA, the E-plane radiation pattern has a narrow half-power beam width of 10°, indicating a high gain characteristic, which is due to the arrangement of the 10 patches along the E-plane. More importantly, due to the uniform loss characteristics of GAF, the radiation sidelobe of GAF LAA is more than 5 dB lower than that of copper antenna. The measured gain of the GAF and copper LAA are shown in Fig. 2(e). The GAF LAA has a maximum gain of 15.75 dBi. The radiation efficiency of GAF and copper LAA at 26 GHz are 83.3% and 90.9%, respectively, as shown in Fig. S4. An efficiency loss of 7% is acceptable for high gain antenna arrays.

3.2. GAF four beam directional scanning phased array antenna

For 5G millimeter wave communications, the high directivity of the antenna can bring benefits of strong signal strength, low noise and great channel capacity (according to Shannon's law). However, in order to achieve omni-directional coverage of base station signals, higher deployment costs will be required. The multi-beam directional scanning antenna is a perfect solution to reduce deployment costs while maintaining channel capacity. To reduce cost and facilitate processing, microstrip Butler matrix is designed to achieved four beam directional scanning phased array antenna (DSPAA). The Butler matrix consists of three parts: quadrature hybrids, crossover and phase shifters. The four quadrature hybrids, two crossover and four phase shifters are reasonably combined to form a four-beam Butler feeding network as shown in Fig. S5. Ports 1–4 are the feeding ports of the Butler matrix, and Ports 5–8 are the corresponding output port connected to the LAA. Each feeding port inputs a signal, and the four output ports will generate four signals with the same power but different phases. Table S2 summarizes the detail of phase changes. Fig. 3(a) is the top view of the microstrip GAF Butler matrix. In order to facilitate impedance matching with LAA, the Butler matrix microstrip line is designed with a characteristic impedance of 100 Ω. Fig. 3(b) shows the simulated results of the phase changes in GAF Butler matrix, which is consistent with the expected design. The proposed GAF DSPAA containing a Butler matrix and four GAF LAAs is shown in Fig. S6. Fig. S7(a) shows the simulated reflection coefficient of Ports 1–4. Due to the symmetry of DSPAA about the *y*-axis direction, the reflection coefficients of Port 1 and Port 2 coincide with Port 4 and Port 3 respectively. The port isolations of DSPAA are shown in Figs. S7(b) and (c). When the ports work individually, the mutual

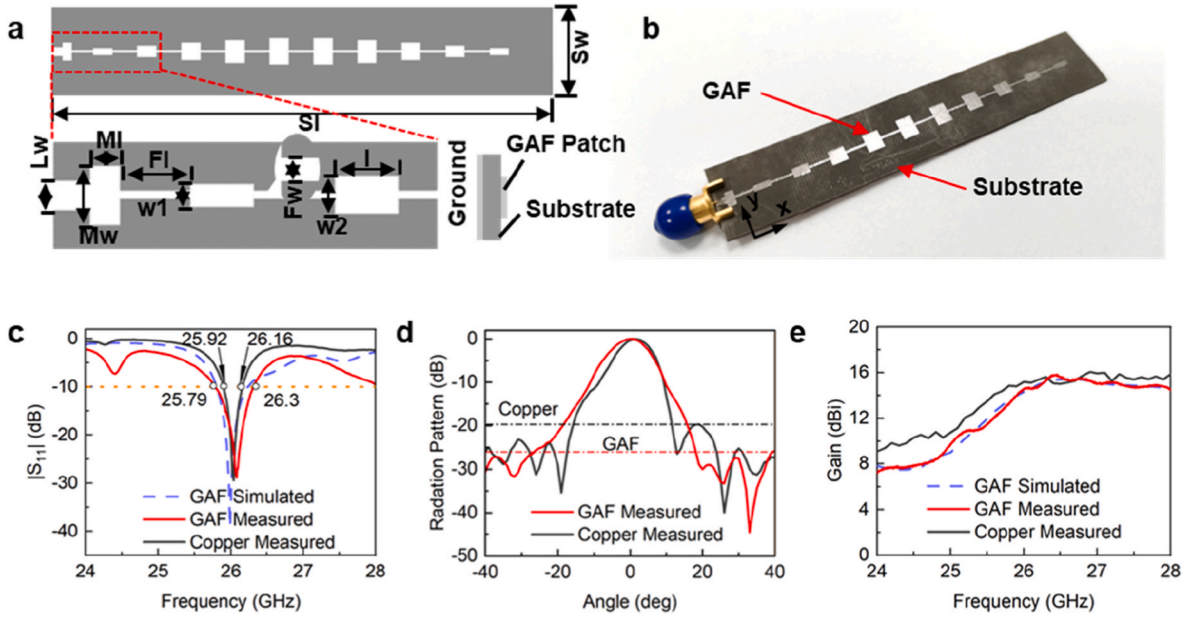

Fig. 2. (a, b) The structure diagram (a) and digital photograph (b) of GAF linear array antenna. (c) Simulated and measured reflection coefficient. (d) Measured E-plane radiation pattern of GAF LAA and copper LAA. (e) Simulated and measured gain of LAA. (A colour version of this figure can be viewed online.)

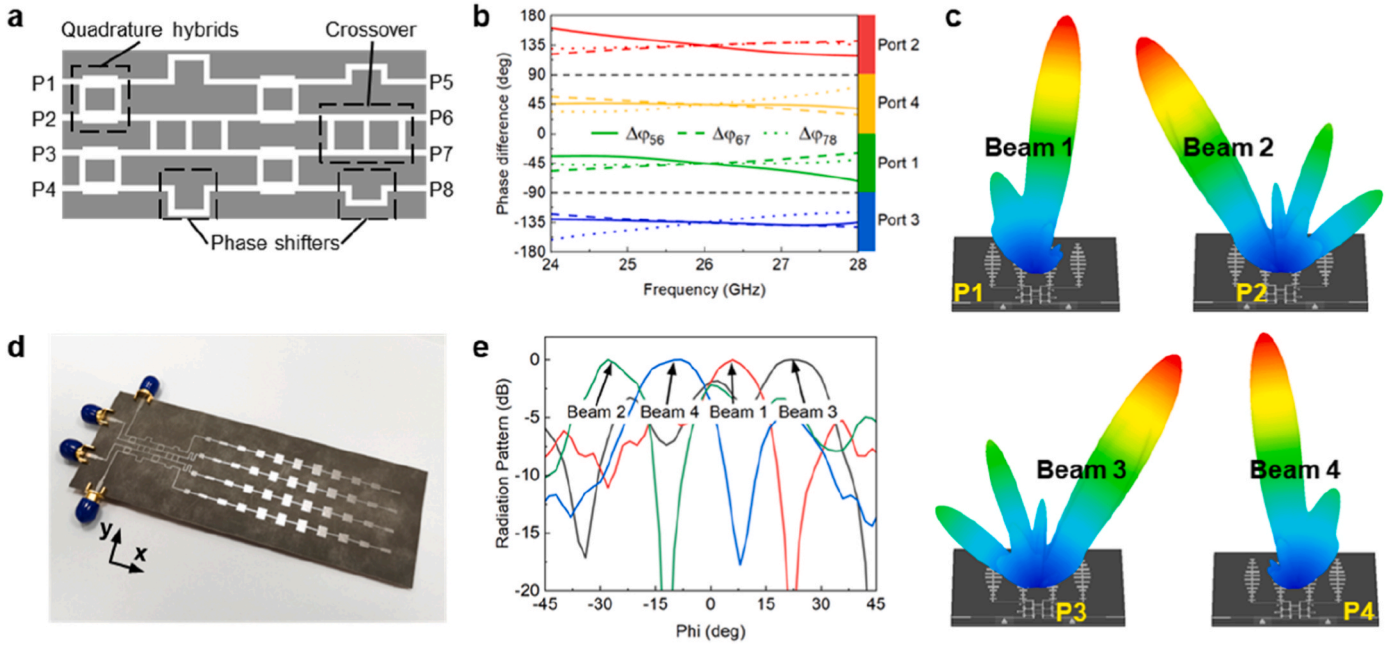

Fig. 3. (a) The structure of microstrip Butler matrix feeding network (P1-4 are the input ports, P5-8 are the output ports). (b) Phase difference of each output port of Butler matrix feeding network. (c) Simulated 3-D radiation patterns with Ports 1–4 excited. (d) Digital photograph of GAF four beam DSPAA. (e) Measured 2-D radiation patterns with different ports activated of GAF DSPAA. (A colour version of this figure can be viewed online.)

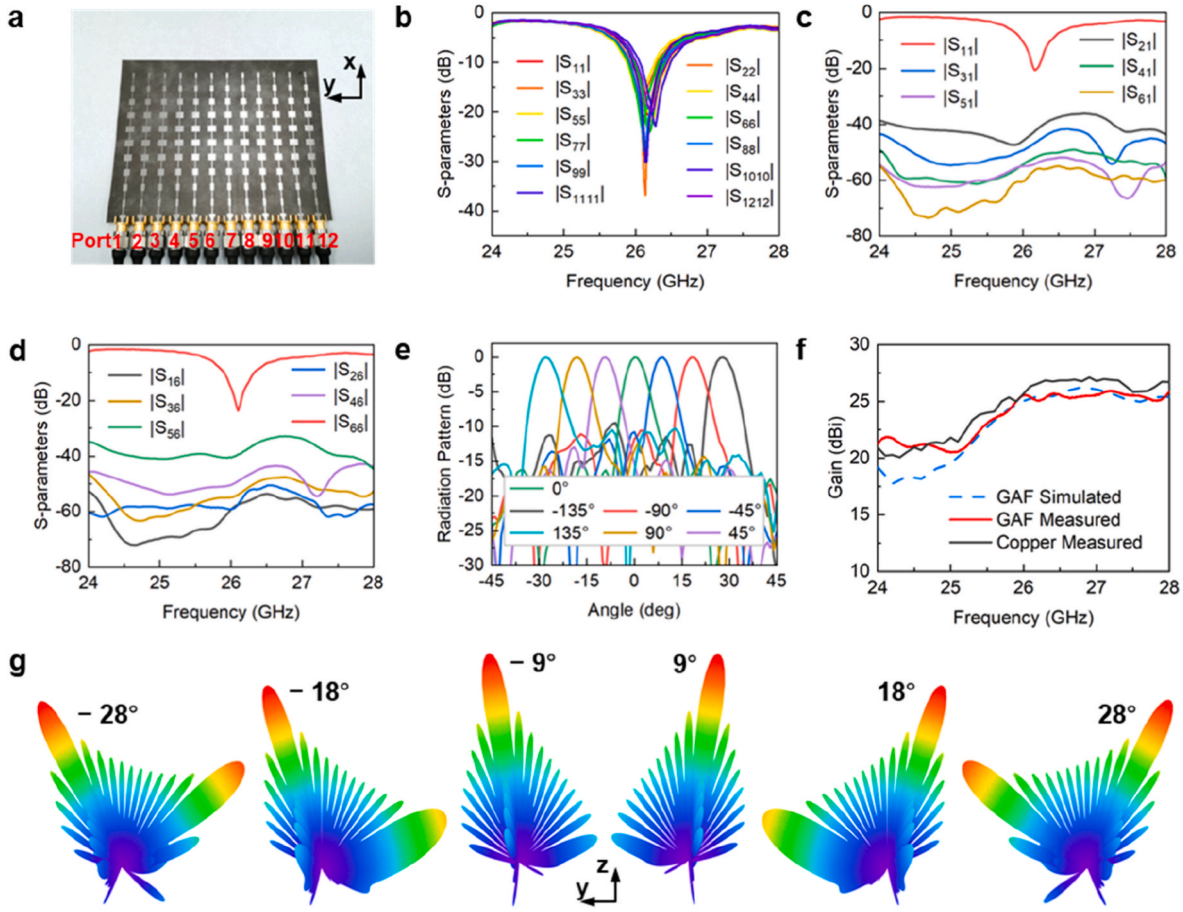

Fig. 4. (a) Digital photograph of the GAF CSPAA. (b–d) Measured reflection coefficients (b) and isolations (c, d) of GAF CSPAA. (e) Measured 2-D radiation pattern at different scanning angles of GAF CSPAA. (f) The simulated and measured gain of CSPAA within the working frequency band. (g) Simulated 3-D radiation pattern when the port phase difference is −135°, −90°, −45°, 45°, 90° and 135°. (A colour version of this figure can be viewed online.)

influence is low. As shown in Fig. 3(c) and Fig. S8, the Beams 1–4 is the simulated radiation patterns when the Ports 1–4 of GAF DSPAA are activated. The maximum radiation of GAF DSPAA points to four directions of −28°, −8°, 8° and 28° respectively. The digital photo of GAF DSPAA and copper DSPAA are shown in Fig. 3(d) and Fig. S9, respectively. As shown the measured reflection coefficients in Figs. S10(a) and (b), the GAF DSPAA has awider impedance bandwidth than copper DSPAA. In addition, the GAF DSPAA has similiar isolations of each ports to the copper DSPAA at 26 GHz, as depicted in Figs. S10(c)–(f). Fig. 3(e) and Fig. S11 is the measured H-plane radiation patterns of GAF DSPAA and copper DSPAA. The four beams of GAF DSPAA point to −28°, −8°, 6° and 22° respectively, which are consistent with the simulated results and copper measured results of −31°, −10°, 11°, 31°.

3.3. GAF continuous scanning phased array antenna

DSPAA can detect and transmit information in several fixed directions by switching mechanism, but lacks the function of continuous beam scanning. Therefore, the GAF continuous scanning phased array antenna (CSPAA) is further designed. The GAF LAA is arranged in the H-plane direction (*y*-axis) at interval of one wavelength to form an array. Fig. 4(a) and Fig. S13 show the digital photo of the GAF CSPAA and copper CSPAA consisting of 12 LAAs, respectively. The position and sequence of the 12 GAF LAAs are marked along the *y*-axis. The measured reflection coefficients of GAF and copper CSPAA are shown in Fig. 4(b) and Fig. S14(a), which match the simulated results in Fig. S12(a). The measured −10 dB impedance bandwidth of Port 1 of GAF CSPAA is 25.98–26.38 GHz, which is 200% of that of copper CSPAA's 26.16–26.36 GHz. In addition, the measured −10 dB impedance bandwidth of port 6 of GAF CSPAA is 210% of that of copper CSPAA, which is consistent with the measured result of LAA. The measured isolations of Port 1 and Port 6 of GAF CSPAA (Fig. 4(c) and (d)) are consistent with the simulated results (Figs. S12(b) and (c)) and copper CSPAA (Figs. S14 (b) and (c)), which indicate that the port spacing is positively correlated with isolation level. The isolation between ports exceeds 35 dB, which ensures that they can work independently without adjacent interference and has a great influence on the increase of channel capacity during wireless signal transmission. Figs. S15(a) and (b) show the schematic diagram and photo of the test environment in microwave anechoic chamber when the radiation performance of CSPAA was under measured. RF signal is generated by vector network analyzer. TMYTEK's BBox can accurately control the phases of the 12 LAAs' input signals independently thus realizing the continuous beam scanning of the GAF CSPAA. Fig. 4(e) and Fig. S14(d) show the measured H-plane radiation pattern of GAF and copper CSPAA at different scanning angles at 26 GHz. It can be clearly seen that when the port feeding phase difference values are −135°, −90°, −45°, 0°, 45°, 90°, 135°, the GAF and copper CSPAA achieves the same beam pointing to 28°, 18°, 9°, 0°, −9°, −18°, −28° respectively with the half-power beam width of 5.3°, which is consistent with the simulated results of Fig. S12(d). It should be pointed out that for the convenience of testing, only a limited number of angles have been selected. In practice, if the feeding phase difference is continuously adjusted, the beam direction will also change continuously. Fig. 4(f) shows the simulated and measured radiation gain of GAF and copper CSPAA between the working frequency band. The GAF CPSAA has a maximum gain of 25.9 dBi, which is only 1.2 dB lower than that of copper. The 3-D radiation pattern can intuitively show the beam direction of the antenna in space. Fig. 4(g) and Fig. S16 show the simulated 3-D radiation patterns at different feeding phase differences. When the phase difference is zero, the radiation direction of GAF CSPAA is perpendicular to the antenna plane (0°). When the phase difference is set to specific values other than zero, CSPAA can obtain continuous beam scanning in different directions from −28° to 28°.

4. Conclusion

In conclusion, this work demonstrates 2 mm-wave phased array antennas based on highly conductive graphene-assembled film. The GAF antennas have good working performance and satisfy the requirements of 5G millimeter wave beamforming technology. Compared with copper antenna, GAF antenna has better working bandwidth and radiation sidelobe performances. The GAF DSPAA has four input ports with four beams pointing to −28°, −8°, 6° and 22° respectively. Furthermore, the GAF CSPAA has a maximum radiation gain of 25.53 dBi at 26 GHz and a narrow half-power beam width of 5.3°, which are similar to the results of copper antenna. By changing the phase difference of input signals, the beam of GAF CSPAA can be continuously scanned within a range of −28°–28°. This research shows a broad application prospect in large-capacity, low-latency, and high-density access that are required for future 5G millimeter wave wireless communications. At the same time, the GAF beamforming technology can also be used for wireless detection and sensing applications of millimeter wave radar.

CRediT authorship contribution statement

Shaoqiu Jiang: Conceptualization, Methodology, Validation, Investigation, Writing – original draft, Writing – review & editing. **Rongguo Song:** Validation, Investigation, Supervision, Writing – original draft, Writing – review & editing. **Zelong Hu:** Investigation, Validation. **Yitong Xin:** Validation. **Guan-Long Huang:** Supervision. **Daping He:** Supervision, Project administration, Funding acquisition, Writing – review & editing.

Declaration of competing interest

The authors declare that they have no known competing financial interests or personal relationships that could have appeared to influence the work reported in this paper.

Acknowledgements

The authors acknowledge financial support from the National Natural Science Foundation of China (51672204, 51701146), Wuhan Application Foundation Frontier Project (Grant No. 2020020601012220) and the Fundamental Research Funds for the Central Universities (WUT: 205209016 and 2020IB005). We also thank the Analytical and Testing Center of Wuhan University of Technology for performing various characterization and measurements.

Appendix A. Supplementary data

Supplementary data to this article can be found online at https://doi.org/10.1016/j.carbon.2022.05.026.

References

[1] W. Lei, A.C.K. Soong, L. Jianghua, W. Yong, B. Classon, W. Xiao, et al., 5G System Design, second ed., Springer, Switzerland, 2021.
[2] B.T. Jijo, S.R. Zeebaree, R.R. Zebari, M.A. Sadeeq, A.B. Sallow, S. Mohsin, et al., A comprehensive survey of 5G mm-wave technology design challenges, Asian J. Res. Comput. Sci. 8 (2021) 1–20.
[3] A.N. Uwaechia, N.M. Mahyuddin, A comprehensive survey on millimeter wave communications for fifth-generation wireless networks: feasibility and challenges, IEEE Access 8 (2020) 62367–62414.
[4] C. Yu, J. Jing, H. Shao, Z.H. Jiang, P. Yan, X. Zhu, et al., Full-angle digital predistortion of 5G millimeter-wave massive MIMO transmitters, IEEE T Microw. Theory 67 (2019) 2847–2860.
[5] Y. Zhao, G. Yu, H. Xu, 6G mobile communication network: vision, challenges and key technologies, Sci. Sin. Inf. 49 (2019) 963–987.
[6] H. Tataria, M. Shafi, A.F. Molisch, M. Dohler, H. Sjöland, F. Tufvesson, 6G wireless systems: vision, requirements, challenges, insights, and opportunities, P IEEE 109 (2021) 1166–1199.

[7] X. You, C. Wang, J. Huang, X. Gao, Z. Zhang, M. Wang, et al., Towards 6G wireless communication networks: vision, enabling technologies, and new paradigm shifts, Sci. China Inf. Sci. 64 (2021) 101–174.
[8] W. Hong, Z.H. Jiang, C. Yu, D. Hou, H. Wang, C. Guo, et al., The role of millimeter-wave technologies in 5G/6G wireless communications, IEEE J. Microw. 1 (2021) 101–122.
[9] H. Jia, L. Kuang, W. Zhu, Z. Wang, F. Ma, Z. Wang, et al., A 77 GHz frequency doubling two-path phased-array FMCW transceiver for automotive radar, IEEE J. Solid-St Circ. 51 (2016) 2299–2311.
[10] J.E. Stailey, K.D. Hondl, Multifunction phased array radar for aircraft and weather surveillance, P IEEE 104 (2016) 649–659.
[11] T. Kinghorn, I. Scott, E. Totten, Recent Advances in Airborne Phased Array Radar Systems, 2016, pp. 1–7.
[12] K. Kibaroglu, M. Sayginer, T. Phelps, G.M. Rebeiz, A 64-element 28-GHz phased-array transceiver with 52-dBm EIRP and 8–12-Gb/s 5G link at 300 meters without any calibration, IEEE T Microw. Theory 66 (2018) 5796–5811.
[13] B. Yu, K. Yang, C. Sim, G. Yang, A novel 28 GHz beam steering array for 5G mobile device with metallic casing application, IEEE T Antenn. Propag. 66 (2018) 462–466.
[14] J. Park, H. Seong, Y.N. Whang, W. Hong, Energy-efficient 5G phased arrays incorporating vertically polarized endfire planar folded slot antenna for mmWave mobile terminals, IEEE T Antenn. Propag. 68 (2020) 230–241.
[15] W. Hong, Z.H. Jiang, C. Yu, J. Zhou, P. Chen, Z. Yu, et al., Multibeam antenna technologies for 5G wireless communications, IEEE T Antenn. Propag. 65 (2017) 6231–6249.
[16] Q. Yang, Z. Li, X. Lu, Q. Duan, L. Huang, J. Bi, A review of soil heavy metal pollution from industrial and agricultural regions in China: pollution and risk assessment, Sci. Total Environ. 642 (2018) 690–700.
[17] K.H. Vardhan, P.S. Kumar, R.C. Panda, A review on heavy metal pollution, toxicity and remedial measures: current trends and future perspectives, J. Mol. Liq. 290 (2019), 111197.
[18] A.K. Awasthi, J. Li, L. Koh, O.A. Ogunseitan, Circular economy and electronic waste, Nat. Elect. 2 (2019) 86–89.
[19] Communiqué: Realizing True Zero, Carbon Neutrality Coalition, 2020.
[20] K.S. Novoselov, A.K. Geim, S.V. Morozov, D. Jiang, Y. Zhang, S.V. Dubonos, et al., Electric field effect in atomically thin carbon films, Science 306 (2004) 666–669.
[21] C. Lee, X. Wei, J.W. Kysar, J. Hone, Measurement of the elastic properties and intrinsic strength of monolayer graphene, Science 321 (2008) 385–388.
[22] X. Du, I. Skachko, A. Barker, E.Y. Andrei, Approaching ballistic transport in suspended graphene, Nat. Nanotechnol. 3 (2008) 491–495.
[23] A.A. Balandin, S. Ghosh, W. Bao, I. Calizo, D. Teweldebrhan, F. Miao, et al., Superior thermal conductivity of single-layer graphene, Nano Lett. 8 (2008) 902–907.
[24] M.V. Kamalakar, C. Groenveld, A. Dankert, S.P. Dash, Long distance spin communication in chemical vapour deposited graphene, Nat. Commun. 6 (2015) 1–8.
[25] A. Pospischil, M. Humer, M.M. Furchi, D. Bachmann, R. Guider, T. Fromherz, et al., CMOS-compatible graphene photodetector covering all optical communication bands, Nat. Photonics 7 (2013) 892–896.
[26] K. Kostarelos, K.S. Novoselov, Exploring the interface of graphene and biology, Science 344 (2014) 261–263.
[27] J. Yao, Y. Sun, M. Yang, Y. Duan, Chemistry, physics and biology of graphene-based nanomaterials: new horizons for sensing, imaging and medicine, J. Mater. Chem. 22 (2012) 14313–14329.
[28] R. Song, Q. Wang, B. Mao, Z. Wang, D. Tang, B. Zhang, et al., Flexible graphite films with high conductivity for radio-frequency antennas, Carbon 130 (2018) 164–169.
[29] S. Li, R. Song, B. Zhang, B. Huang, X. Zhao, D. He, Wearable near-field communication bracelet based on highly conductive graphene-assembled films, Int. J. RF Microw. Computer-Aided Eng. 31 (2021), e22479.
[30] R. Song, Z. Wang, H. Zu, Q. Chen, B. Mao, Z.P. Wu, et al., Wideband and low sidelobe graphene antenna array for 5G applications, Sci. Bull. 66 (2021) 103–106.
[31] D. Tang, Q. Wang, Z. Wang, Q. Liu, B. Zhang, D. He, et al., Highly sensitive wearable sensor based on a flexible multi-layer graphene film antenna, Sci. Bull. 63 (2018) 574–579.
[32] Z. Hu, Z. Xiao, S. Jiang, R. Song, D. He, A dual-band conformal antenna based on highly conductive graphene-assembled films for 5G WLAN applications, Materials 14 (2021) 5087.
[33] C. Fan, B. Wu, R. Song, Y. Zhao, Y. Zhang, D. He, Electromagnetic shielding and multi-beam radiation with high conductivity multilayer graphene film, Carbon 155 (2019) 506–513.